ASCE

Simplified Nonlinear Simulation of Rectangular Concrete-Filled Steel Tubular Columns

Zhong Tao, M.ASCE[1]; Utsab Katwal[2]; Brian Uy, F.ASCE[3]; and Wen-Da Wang, M.ASCE[4]

Abstract: In detailed three-dimensional (3D) finite-element modeling, two-dimensional and/or 3D elements are widely used because of their high accuracy and ease of use despite the high computational cost. In contrast, simplified modeling based on fiber beam element (FBE) formulation is preferred for developing macro models to simulate structural frames due to its simplicity and computational efficiency. As for the FBE simulation of concrete-filled steel tubular (CFST) columns, its accuracy largely depends on the input steel and concrete material models, which should implicitly consider the material nonlinearity and interaction between the steel and concrete components. The authors have previously developed a FBE model for circular CFST columns, and this paper is a continuation of the previous work. In this paper, uniaxial effective stress–strain relationships are developed for the steel and concrete materials in rectangular CFST columns based on rigorous analysis of data generated from 3D finite-element modeling of stub columns. Thus, the material models have implicitly considered the effects of yielding and local buckling of the steel tube and passive confinement to the concrete. Meanwhile, the size effect is also considered in the concrete model. The accuracy of the proposed material models is verified against a database of rectangular CFST stub columns covering a wide range of material and geometric parameters. The developed material models are further used to simulate rectangular CFST slender columns and beam-columns, and a reasonably good agreement is achieved between the experimental and predicted load–deformation curves. **DOI: 10.1061/(ASCE)ST.1943-541X.0003021.**

Author keywords: Concrete-filled steel tubes (CFST); Simplified simulation; Fiber beam element model; Concrete confinement; Local buckling; Size effect.

Introduction

Concrete-filled steel tubular (CFST) columns are currently widely used in construction because of the excellent composite action between the steel tube and core concrete. The composite columns also provide economic benefits, as the need for concrete formwork is eliminated during construction (Han et al. 2014). In practice, three types of CFST columns are dominantly used, i.e., circular, square, and rectangular columns. For simplicity of description, a square section is considered as a special case of a rectangular section in the following, unless otherwise specified. Although circular CFST columns generally provide better confinement to the core concrete than rectangular CFST columns, the latter are still widely used in construction due to their large bending stiffness, ease of connection to beams, and aesthetic considerations (Han et al. 2014).

Three-dimensional (3D) finite-element (FE) modeling has been widely adopted to simulate CFST members (Tao et al. 2013b). However, developing 3D FE modeling is quite tedious, especially for the routine analysis and design of structural frames. In contrast, simplified numerical modeling such as fiber beam element (FBE) modeling is known for its simplicity and high computational efficiency, and thus is preferred for developing macro models to simulate structural frames for routine design. Particularly, the FBE model might be directly used in the design of frames using advanced analysis, as the real strength of structural frames can be easily evaluated (Zhang and Rasmussen 2013).

However, the interaction between the steel tube and concrete in CFST columns cannot be directly captured by a FBE model. Therefore, the accuracy of such FBE modeling is greatly affected by the accuracy of the input uniaxial material models, which should implicitly consider the material nonlinearity and the interaction between the steel and concrete components, such as the yielding and local buckling of the steel tube and passive confinement to the concrete. Furthermore, rectangular CFST columns tend to demonstrate a size effect due to the relatively weak confinement to concrete. Based on experimental results, Sakino et al. (2004) proposed a simple equation to consider size effect for CFST columns. It should be pointed out that existing tests were mostly conducted on rectangular columns with cross-sectional depths less than 320 mm except those conducted by Chen et al. (2012) and Wu et al. (2018). Chen et al. (2012) tested square columns with cross-sectional widths up to 500 mm. They suggested that the section size may have an influence on the stress–strain curve of core concrete. Wu et al. (2018) tested six square CFST stub columns under axial compression to further confirm the size effects, where the cross-sectional dimensions of the columns are in the range of 300–750 mm. All the columns have the same B/t ratio of 50, where B and t are the overall width and thickness of the tube, respectively. The concrete cylinder compressive strength (f'_c) is 27.9 MPa and the yield stress of the steel tube (f_y) varies from 302 to 334 MPa. For columns with a cross-sectional size of 300 mm, the measured ultimate strength is 11% higher than the simple summation (P_0) of the strength of the

[1]Professor, Centre for Infrastructure Engineering, Western Sydney Univ., Penrith, NSW 2751, Australia (corresponding author). ORCID: https://orcid.org/0000-0003-2117-2162. Email: z.tao@westernsydney.edu.au

[2]Postdoctoral Research Associate, School of Civil Engineering, Univ. of Sydney, Sydney, NSW 2006, Australia. Email: utsab.katwal@sydney.edu.au

[3]Professor, School of Civil Engineering, Univ. of Sydney, Sydney, NSW 2006, Australia. Email: brian.uy@sydney.edu.au

[4]Professor, School of Civil Engineering, Lanzhou Univ. of Technology, Lanzhou 730050, China. ORCID: https://orcid.org/0000-0001-6735-9171. Email: wangwd@lut.edu.cn

Note. This manuscript was submitted on September 16, 2020; approved on January 25, 2021; published online on March 24, 2021. Discussion period open until August 24, 2021; separate discussions must be submitted for individual papers. This paper is part of the ***Journal of Structural Engineering***, © ASCE, ISSN 0733-9445.

steel section and that of the concrete core. However, the ultimate strength is 10% lower than P_0 when the cross-sectional size increases to 750 mm, which further confirms the clear size effect (Wu et al. 2018). The review highlights that the size effect should also be considered in developing material models for FBE modeling of rectangular CFST columns.

There are a few material models available in the literature for FBE simulation of square and/or rectangular CFST columns (Sakino et al. 2004; Liang et al. 2006; Thai et al. 2015; Lai and Varma 2016). Sakino et al. (2004) developed empirical material models for square CFST stub columns, but their models were only verified by their own test data. Their concrete model considered the influence of size effect, but the strength reduction factor was derived from limited test data of unconfined concrete. Meanwhile, their steel model implicitly considered the local buckling effect but adopted an oversimplified multilinear stress–strain ($\sigma - \varepsilon$) relationship. Liang et al. (2006) and Thai et al. (2015) also developed empirical material models for square and/or rectangular CFST stub columns. The local buckling effect was explicitly considered in the steel model, which is not favorable to be used in macro models. Meanwhile, the size effect was not considered in their models. Lai and Varma (2016) developed effective material $\sigma - \varepsilon$ models using detailed 3D FE modeling as a tool. Potentially, the developed $\sigma - \varepsilon$ models can reflect the real interaction between the steel tube and concrete, provided that the 3D FE model has been extensively validated. However, Lai and Varma (2016) only specifically developed material models for noncompact and slender CFST columns, which might not be suitable for columns with compact sections. Meanwhile, the size effect of rectangular CFST columns is also not considered in their material models. The literature review has clearly identified a research need to develop accurate uniaxial effective steel and concrete models for FBE simulation of rectangular CFST columns.

Katwal et al. (2017) recently proposed effective material $\sigma - \varepsilon$ models for the simplified FBE modeling of circular CFST columns, in which the 3D FE model developed by Tao et al. (2013b) was used to assist the development. The previous work conducted by Katwal et al. (2017) will be further extended in this paper to develop similar effective steel and concrete $\sigma - \varepsilon$ models for rectangular CFST columns through rigorous analysis of data generated from 3D FE modeling of stub columns. Meanwhile, the size effect will be considered in the concrete model. The accuracy of the proposed material models will be further verified against an experimental database of rectangular CFST stub columns covering a wide range of material and geometric parameters. The developed material models will be subsequently used to simulate slender rectangular CFST columns and beam-columns. It is expected that the proposed material models might be directly incorporated into commercial software to improve the simulation accuracy of CFST members. Meanwhile, the proposed material models may also be used by engineers to perform preliminary analysis of CFST members by using a spreadsheet.

Numerical Modeling

3D FE Modeling

The 3D FE model developed by Tao et al. (2013b) has been successfully used by Katwal et al. (2017) to generate numerical data for circular CFST stub columns. By analyzing the numerical data, Katwal et al. (2017) developed effective $\sigma - \varepsilon$ models for FBE modeling of circular CFST stub columns. The accuracy of the FBE modeling was then verified by comparing the predicted load–deformation curves with experimental curves. The approach adopted by Katwal et al. (2017) has been proved to be successful, and therefore is also used in this study to develop effective $\sigma - \varepsilon$ material models for rectangular CFST columns. Details of the approach will be shown in the following subsections.

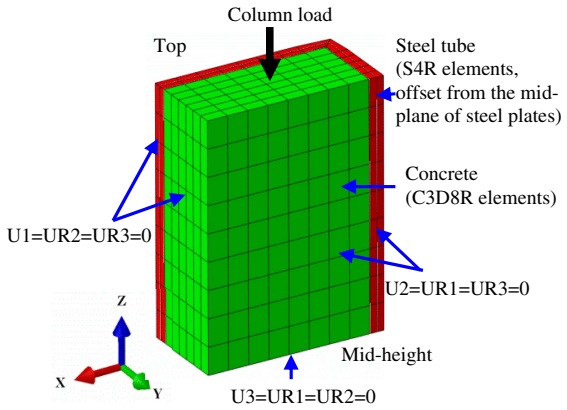

Fig. 1. Typical one-eighth model used in 3D FE simulation of rectangular CFST columns.

In this study, numerical data were first generated using the ABAQUS version 6.12–based 3D FE model developed by Tao et al. (2013b) for rectangular CFST stub columns subjected to axial compression. The length of a stub column was chosen to be three times the overall depth of the cross section. In the 3D FE modeling, solid elements (C3D8R) were used to simulate core concrete, whereas shell elements (S4R) were used to simulate the steel tube. In using shell elements, the reference plane of the elements should be defined, and it was chosen to be the midplane of the steel plate in this study. To increase computational efficiency, one-eighth FE models were built, and symmetric boundary conditions were applied to the symmetric planes, as shown in Fig. 1. According to Tao et al. (2013b), the elastic-perfectly plastic $\sigma - \varepsilon$ model was utilized for the simulation of steel tubes, whereas the $\sigma - \varepsilon$ model proposed by Tao et al. (2013b) was used to simulate core concrete under passive confinement. It should be noted that high strength steel may exhibit continuous yielding without a yield plateau. The adoption of the elastic-perfectly plastic $\sigma - \varepsilon$ model might slightly overestimate the stiffness beyond the steel proportional limit. However, it is expected that the overall influence on the load–deformation curve of a CFST column is not significant. Therefore, the elastic-perfectly plastic steel model is still tentatively used in simulating CFST columns made with high strength steel, although further studies can be conducted to develop more accurate models. It should be noted that local imperfections and residual stresses are not considered in the 3D FE model due to their negligible influence (Tao et al. 2009, 2013b; Thai et al. 2014). Further information about the 3D FE modeling of rectangular CFST stub columns can be found in Tao et al. (2013b).

FBE Modeling

To conduct FBE modeling in ABAQUS version 6.12, two-node linear beam elements (B21) were utilized to define the core concrete, whereas the steel tube was represented using the *rebar option. Unlike the symmetrical 3D FE models, full models were developed for FBE modeling, as computational time is not an issue for this type of simulation. It should be pointed out that FBE models were developed not only for short columns but also for slender columns in this paper. The influence of cross-section discretization on the prediction

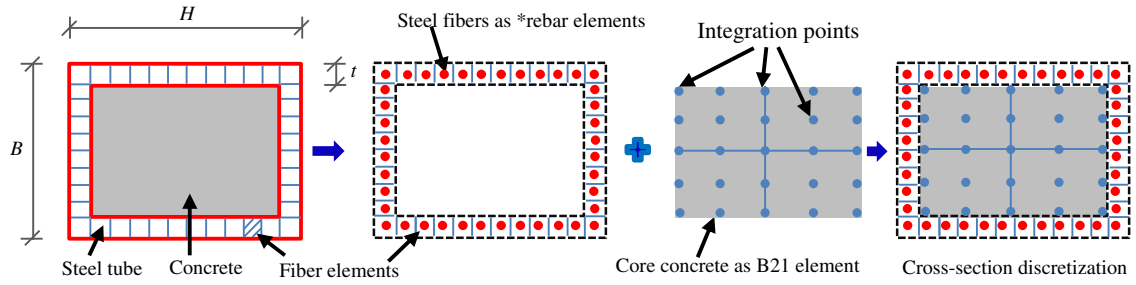

Fig. 2. Discretization of cross section for FBE modeling of rectangular CFST columns.

accuracy of rectangular CFST columns was checked through sensitivity analysis. It was found that the results were not sensitive to section discretization, which is consistent with the findings presented by Katwal et al. (2017) for circular CFST columns. Therefore, the linear beam elements for the core concrete adopted the default 25 integration points in the cross section, whereas the steel tube was divided into 40 longitudinal fiber elements, as shown in Fig. 2. In the axial direction, the CFST column was partitioned into at least ten elements with a maximum size of 100 mm.

No direct interaction can be defined between the steel tube and concrete in FBE modeling. Therefore, it is very important to use effective uniaxial steel and concrete $\sigma - \varepsilon$ models, which must implicitly consider the interaction effect to obtain accurate simulation. It is expected that the steel model for FBE modeling should be able to consider the strength reduction in the axial direction to reflect the influence of possible hoop stress resulting from the lateral expansion of the concrete. Meanwhile, steel yielding and influence of local buckling should also be considered. As for the concrete model for FBE modeling, it should be able to capture the enhancement of strength and ductility due to the passive confinement from the steel tube. One of the major objectives of this paper is to develop such material models for rectangular CFST columns, which will be presented in the following section. The effective steel and concrete $\sigma - \varepsilon$ curves were then incorporated in ABAQUS through a user material (UMAT) subroutine in Fortran language based on the Intel Fortran Compiler version 11.1 platform.

Two-dimensional FBE models were built in the x, y-plane. For axially loaded stub columns, the bottom node was restrained along all degree of freedoms (U1 = U2 = UR3 = 0), whereas the top node was restrained only for the translational degree of freedom along the x-axis (U1 = 0). The load was applied to the top node using a displacement control approach and the analysis was conducted using a static general method. Boundary conditions and consideration of imperfections for slender columns and beam-columns will be presented later. Further information about the assumptions made in FBE modeling and the procedure to develop the FBE model can be found in Katwal et al. (2017).

Development of Material Models for FBE Modeling

Interaction between the steel tube and concrete is expected to occur in a rectangular CFST column at some stage (Tao et al. 2013b). Confinement from a rectangular steel tube might have a small influence on the strength of concrete but can significantly increase its ductility. Such interaction is dependent on various column parameters, such as yield stress of steel (f_y), unconfined concrete cylinder strength (f'_c), width-to-thickness ratio, and depth-to-width ratio. The interaction can also lead to the development of tensile hoop stress in the steel tube, thus reducing the load-bearing capacity in the longitudinal direction (Sakino et al. 2004). To capture the complex mechanism of interaction between the steel tube and concrete, it would be advantageous to use the advanced 3D FE modeling developed by Tao et al. (2013b), which has been rigorously verified by numerous experimental data.

Two groups of numerical data are generated using the 3D FE model. The first group of data is generated from the simulation of 183 test specimens of rectangular stub columns, as summarized in Table 1. The overall cross-sectional depths (H) of the test specimens are in the range of 60–750 mm, showing that the specimens have a wide range of sizes. The experimental axial load–axial strain ($N - \varepsilon$) curves are later used to verify the developed effective material models. However, the material and geometric parameters of most experimental data are concentrated in a narrow range. Therefore, the second group of numerical data is generated from parametric analysis of 192 stub columns to cover a wide range of parameters, including yield stress of steel (f_y = 200, 460, 690, and 960 MPa), concrete compressive strength (f'_c = 20, 50, 100, and 200 MPa), cross-sectional aspect ratio (H/B = 1, 1.5, and 2), and B/t ratio (12, 52, 100, and 150). The ranges of parameters are selected based on the test data and practical ranges in the construction of CFST columns. It is worth noting that sometimes a small extrapolation has been made to the current limit of a parameter. For example, the 3D FE model proposed by Tao et al. (2013b) was only validated by test data of CFST columns with f'_c up to 185 MPa. In this paper, the upper limit of f'_c is chosen to be 200 MPa in the parametric analysis. Further research is required to justify the extrapolation. In the analyses, all combinations of the four parameters are considered. It should be mentioned that B of the samples is taken as a constant value of 400 mm. This is because the 3D FE model developed by Tao et al. (2013b) did not consider size effect. Although some recent efforts have been made by Lin and Zhao (2019) to consider size effect in 3D FE modeling of circular CFST stub columns, no such models are available for rectangular CFST stub columns. This is due to the fact that the size effect of rectangular CFST columns is more complicated than that of circular counterparts due to the uneven concrete confinement in a rectangular cross section. Further research is required to develop a reliable 3D FE model to consider size effect for rectangular CFST columns. In this paper, size effect will be tentatively considered by introducing an empirical factor in the concrete model and calibrated against the test data summarized in Table 1.

After the 3D FE modeling, the force resisted by the steel tube/core concrete at the midheight of the column is then divided by the corresponding cross-sectional area to generate the averaged steel/concrete $\sigma - \varepsilon$ curve, which is the uniaxial effective $\sigma - \varepsilon$ curve required for FBE modeling. Based on the numerical data obtained from the 3D FE modeling, regression analysis is then performed to develop effective steel and concrete $\sigma - \varepsilon$ models, which will be described in the following subsections.

Table 1. Summary of test data for rectangular CFST stub columns

Number of specimens	B (mm)	H (mm)	t (mm)	H/B	B/t	L/B	f_y (MPa)	f'_c (MPa)	Source
9	150	150	2.0–4.3	1.0	35–75	3.0	294–341	18–35	Tomii et al. (1977)
4	152	152–254	4.4–9.0	1.0–1.7	17–41	1.8–3.0	377–432	45–49	Lu and Kennedy (1992)
4	80–239	80–239	2.1	1.0	37–112	3.4–3.5	282	17–19	O'Shea and Bridge (1997)
11	77–127	127–153	3.0–7.5	1.0–2.0	17–51	4.0–4.8	312–430	24–30	Schneider (1998)
3	156–306	156–306	3.0	1.0	52–102	2.9	300	38–50	Uy (2000)
4	305	305	5.8–8.9	1.0	34–53	3.9	259–660	110	Varma (2000)
6	100–301	100–301	2.2–6.1	1.0	46–49	3.0	300–395	26–58	Yamamoto et al. (2000)
20	120–200	120–200	3.8–5.9	1.0	20–36	3.0	321–330	13–46	Han et al. (2001)
18	70–135	90–160	2.9–7.6	1.0–1.8	21–52	3.0	194–228	50	Han (2002)
3	200–300	200–300	2.0–5.0	1.0	40–150	3.0	266–342	27–31	Huang et al. (2002)
8	80–182	100–182	4.2	1.0–2.0	24–44	3.0	550	61–72	Liu et al. (2003)
2	200	200	3	1.0	66	3.0	303.5	49.5	Han and Yao (2004)
9	100–101	100–101	4.0–10.0	1.0	10–24	3.0	289–400	25–89	Lam and Williams (2004)
6	119–323	119–323	4.4–6.5	1.0	18–74	3.0	262–835	39–78	Sakino et al. (2004)
24	60–250	60–250	1.9–2	1.0	30–134	3.0	282–404	42–71	Han et al. (2005)
6	80–120	106–180	4.0	1.0–2.0	27–45	3.0	495	60–89	Liu (2005)
10	100–120	120–180	6	1.0–1.8	21–31	3.0	300	83–106	Liu and Gho (2005)
2	129–250	129–250	2.5	1.0	51–100	3.0	234	50–52	Tao et al. (2005)
6	190–250	190–250	2.5	1.0	76–100	3.0	270–342	49–57	Tao et al. (2008)
2	250	250	2.5	1.0	100	3.0	338	20–42	Tao et al. (2009)
4	410–500	410–500	10–16	1.0	26–50	3.0	358–389	43	Chen et al. (2012)
9	150	150	8–12.5	1.0	12–19	3.0	446–779	144–159	Xiong et al. (2017)
6	300–750	300–750	6–15	1.0	50	3.0	302–334	28	Wu et al. (2018)
7	100	100	4.9–18.5	1.0	5–20	3.0	444–646	89–128	Yan et al. (2019)

Material Model of Steel

Characteristics of Effective Stress–Strain Curves for Steel

Parametric analysis shows that the shape of effective $\sigma - \varepsilon$ curves is strongly affected by the confinement factor ξ_c. This factor is defined as $\xi_c = A_s f_y / A_c f'_c$, where A_s and A_c are the cross-sectional areas of the steel tube and concrete, respectively (Tao et al. 2013b). It should be noted that the definition of ξ_c is slightly different from the definition of a similar factor ξ in Han et al. (2014). In defining ξ, f_{ck} is used instead of f'_c, where f_{ck} is taken as $0.67 f_{cu}$ for normal strength concrete, and f_{cu} is the concrete cube compressive strength. It should be noted that both ξ and ξ_c have similar physical meanings. However, ξ_c is used in this paper for two reasons: (1) in many countries (i.e., Australia, Japan, European countries, and the US), f'_c is commonly used to determine the compressive strength of concrete; and (2) f_{ck} for high strength concrete is not readily available. The influence of ξ_c on the effective $\sigma - \varepsilon$ curves of steel is shown in Fig. 3(a). Although the same input $\sigma - \varepsilon$ curve has been used for all columns, the effective $\sigma - \varepsilon$ curves obtained from the 3D FE modeling are quite different from each other and highly dependent on the value of ξ_c. This is due to the combined effects of hoop stresses and local buckling of the steel tube. The large difference in the shape of curves shown in Fig. 3(a) highlights the need to develop an effective $\sigma - \varepsilon$ model of steel for the FBE modeling of rectangular CFST columns.

As depicted in Fig. 3(a), the effective $\sigma - \varepsilon$ curves of steel in rectangular CFST columns demonstrate a linear response in the elastic stage due to the initial weak steel-concrete interaction (Han et al. 2014). After reaching the peak stress, a strong interaction starts to develop and the effective $\sigma - \varepsilon$ curves enter the postpeak stage. Depending on the ξ_c value, the descending slopes of the curves are different. The smaller the ξ_c value, the faster the curve declines. A similar observation has been reported by Katwal et al. (2017) for circular CFST stub columns, which can be explained by the dilation effect of the infill concrete and the localized buckling of the steel tube. For circular CFST stub columns, strain-hardening was observed beyond the critical point $(\varepsilon'_{cr}, f'_{cr}/f_y)$ on the curve

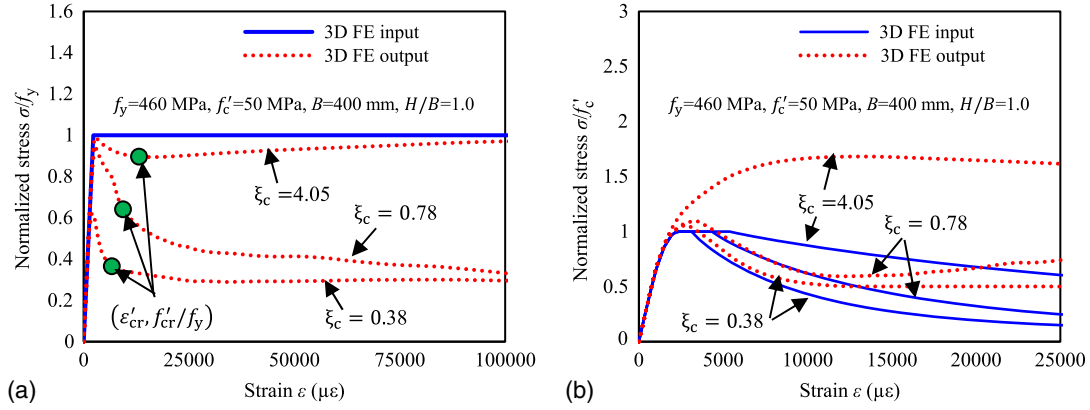

Fig. 3. Effective $\sigma - \varepsilon$ curves of steel and concrete: (a) steel $\sigma - \varepsilon$ curves; and (b) concrete $\sigma - \varepsilon$ curves.

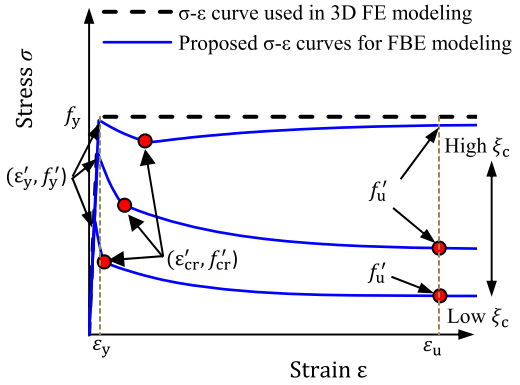

Fig. 4. Proposed steel $\sigma - \varepsilon$ model for FBE modeling of rectangular CFST columns.

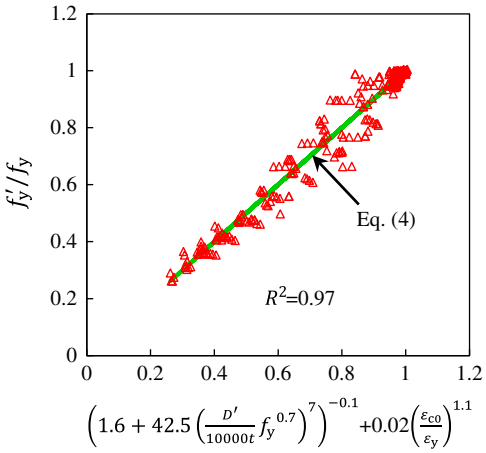

Fig. 5. Verification of proposed equation for f'_y.

in all cases (Katwal et al. 2017). However, for rectangular CFST stub columns, only very stocky columns [such as the one with ξ_c of 4.05 shown in Fig. 3(a)] demonstrate slight strength recovery beyond the critical point. For rectangular columns with ξ_c less than 2, continuous strain softening is observed after the peak stress. This trend is different from that in circular CFST stub columns, because the steel tubes in rectangular CFST columns are more susceptible to local buckling compared to the steel tubes in the circular counterparts (Han et al. 2014). In general, the idealized trilinear model proposed by Lai and Varma (2016) oversimplified the effective steel $\sigma - \varepsilon$ curves for rectangular CFST columns.

Proposed Effective Steel Stress–Strain Relationship

The effective $\sigma - \varepsilon$ curve of steel expressed by Eq. (1) was originally proposed by Katwal et al. (2017) for circular CFST columns. It is found that Eq. (1) can still be used for rectangular CFST columns if the parameters in the equation are recalibrated using the numerical data of rectangular CFST stub columns. A total of six parameters are required to determine key characteristic points on the effective $\sigma - \varepsilon$ curves, as shown in Fig. 4. These parameters include the initial peak stress of steel (f'_y), critical stress (f'_{cr}), critical strain (ε'_{cr}), effective stress (f'_u) corresponding to the ultimate strain of steel (ε_u), and strain softening/hardening exponents ψ and p. These six parameters need to be determined or recalibrated for steel tubes in rectangular columns, which are described in subsections below

$$\sigma = \begin{cases} E_s\varepsilon & 0 \le \varepsilon < \varepsilon'_y \\ f'_{cr} - (f'_{cr} - f'_y)\cdot\left(\dfrac{\varepsilon'_{cr} - \varepsilon}{\varepsilon'_{cr} - \varepsilon'_y}\right)^{\psi} & \varepsilon'_y \le \varepsilon < \varepsilon'_{cr} \\ f'_u - (f'_u - f'_{cr})\cdot\left(\dfrac{\varepsilon_u - \varepsilon}{\varepsilon_u - \varepsilon'_{cr}}\right)^{p} & \varepsilon'_{cr} \le \varepsilon < \varepsilon_u \\ f'_u & \varepsilon \ge \varepsilon_u \end{cases} \quad (1)$$

where E_s = modulus of elasticity of steel, taken as 200,000 MPa if no measured value was reported; ε'_y = strain corresponding to f'_y, taken as f'_y/E_s; and ε_u = ultimate strain of steel corresponding to the ultimate strength (f_u), which can be determined by Eq. (2) suggested by Katwal et al. (2017)

$$\varepsilon_u = \begin{cases} 100\varepsilon_y & f_y \le 300 \text{ MPa} \\ [100 - 0.15(f_y - 300)]\varepsilon_y & 300 < f_y \le 800 \text{ MPa} \\ [25 - 0.1(f_y - 800)]\varepsilon_y & 800 < f_y \le 960 \text{ MPa} \end{cases} \quad (2)$$

where ε_y = yield strain of steel corresponding to the yield stress, taken as f_y/E_s.

Initial Peak Stress f'_y

The ratio of f'_y/f_y represents the initial intensity of the interaction between the steel tube and concrete in CFST columns (Katwal et al. 2017). From the numerical analysis, it is found that the ratio of f'_y/f_y is primarily affected by the ratios of $\varepsilon_y/\varepsilon_{c0}$ and D'/t, where ε_{c0} is the strain corresponding to the peak stress of unconfined concrete. The value of ε_{c0} can be determined from Eq. (3) suggested by De Nicolo et al. (1994). D' is the diagonal distance ($\sqrt{B^2 + H^2}$) between the outer corners of the cross section of the rectangular steel tube

$$\varepsilon_{c0} = 0.00076 + \sqrt{(0.626f'_c - 4.33)\times 10^{-7}} \quad (3)$$

where the unit of f'_c is MPa.

In general, the ratio of f'_y/f_y decreases with increasing $\varepsilon_y/\varepsilon_{c0}$ ratio. This is because a smaller $\varepsilon_y/\varepsilon_{c0}$ ratio leads to a weaker initial interaction because of a delayed initiation of concrete dilation (Katwal et al. 2017). Similarly, f'_y/f_y decreases with an increasing D'/t ratio. Parametric analysis indicates that f'_y/f_y decreases more significantly when the D'/t ratio exceeds 60. This is obvious because the specimens with very large D'/t ratios are more susceptible to local buckling, which might occur at a low load level. By performing a regression analysis of the numerical data, Eq. (4) is proposed to predict f'_y/f_y. The coefficient of determination (R^2) is 0.97, which represents excellent agreement (Fig. 5)

$$\frac{f'_y}{f_y} = \left(1.6 + 42.5\left(\frac{D'}{10{,}000t}f_y^{0.7}\right)^7\right)^{-0.1} + 0.02\left(\frac{\varepsilon_{c0}}{\varepsilon_y}\right)^{1.1} \le 1 \quad \text{and} \quad > 0 \quad (4)$$

Critical Stress f'_{cr} and Critical Strain ε'_{cr}

Based on the data generated from the FE analysis, the ratio of critical stress (f'_{cr}) to the yield stress of steel (f_y) has been found to be primarily affected by ξ_c and the D'/t ratio. When ξ_c increases to approximately 0.5, f'_{cr}/f_y increases almost linearly to 0.75. When ξ_c is above 0.5, f'_{cr}/f_y increases slowly with increasing ξ_c. The smaller the value of ξ_c, the quicker the concrete dilates. For the same reason, f'_{cr}/f_y decreases linearly when D'/t increases. To achieve the highest prediction accuracy of f'_{cr}/f_y, however, ξ_c is

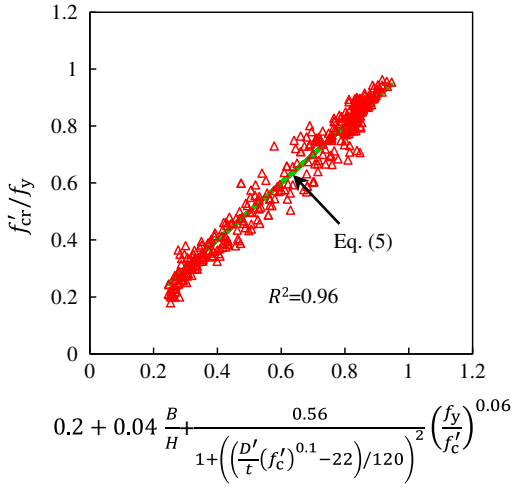

Fig. 6. Verification of proposed equation for f'_{cr}.

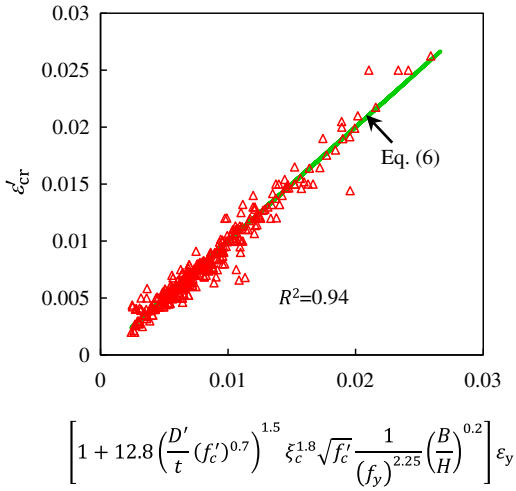

Fig. 7. Verification of proposed equation for ε'_{cr}.

not directly used in regression analysis. Instead, the effects of B/H, D'/t, f'_c, and f_y/f'_c are considered by thoroughly analyzing the numerical data. Through regression analysis, Eq. (5) is proposed to predict f'_{cr}/f_y, and the prediction accuracy is demonstrated in Fig. 6. The value of R^2 is 0.96, which indicates a very good correlation

$$\frac{f'_{cr}}{f_y}=0.2+0.04\frac{B}{H}+\frac{0.56}{1+((\frac{D'}{t}(f'_c)^{0.1}-22)/120)^2}\left(\frac{f_y}{f'_c}\right)^{0.06}$$
$$>0 \text{ and } \le f'_y/f_y \tag{5}$$

The critical strain (ε'_{cr}) is also found to be mainly affected by ξ_c and the D'/t ratio. However, the inclusion of the aspect ratio (B/H), f'_c, and f_y in the prediction model can further improve its accuracy. Accordingly, Eq. (6) is proposed to determine ε'_{cr} based on regression analysis. A very good fit ($R^2=0.94$) is obtained, as shown in Fig. 7

$$\varepsilon'_{cr}=\varepsilon_y\left[1+12.8\left(\frac{D'}{t}(f'_c)^{0.7}\right)^{1.5}\xi_c^{1.8}\sqrt{f'_c}\frac{1}{(f_y)^{2.25}}\left(\frac{B}{H}\right)^{0.2}\right]$$
$$>\varepsilon_y \text{ and } \le \varepsilon_u \tag{6}$$

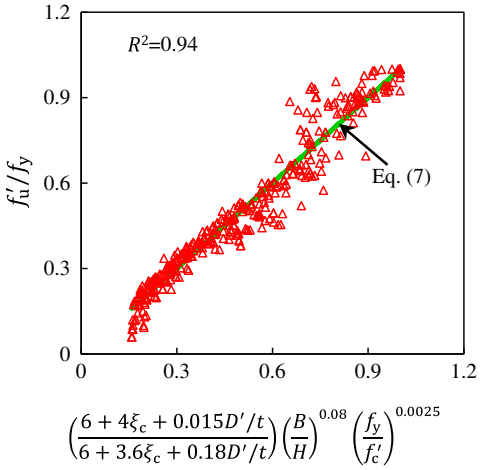

Fig. 8. Verification of proposed equation for f'_u.

Stress f'_u

The effective stress (f'_u) corresponding to the ultimate steel strain (ε_u) is smaller than the yield stress (f_y) owing to the development of transverse stress in the steel tube (Katwal et al. 2017) and possible local buckling. It is found that the factors affecting f'_{cr} also affect f'_u. Accordingly, Eq. (7) is proposed to predict the value of f'_u. Fig. 8 shows the prediction accuracy, indicating a very good correlation ($R^2=0.94$)

$$f'_u=f_y\left(\frac{6+4\xi_c+0.015D'/t}{6+3.6\xi_c+0.18D'/t}\right)\left(\frac{B}{H}\right)^{0.08}\left(\frac{f_y}{f'_c}\right)^{0.0025} \tag{7}$$

Exponents Ψ and p

The value of the strain softening exponent (ψ) was suggested to be 1.5 by Katwal et al. (2017) for circular CFST columns. This value is also found to be applicable to rectangular CFST columns. The exponent (p) was originally used by Tao et al. (2013a) to represent the strain-hardening rate of steel. This exponent p is recalibrated and expressed by Eq. (8) to represent both strength recovery of steel for stocky columns and strain softening beyond the critical point for other columns

$$p=\begin{cases}0.004E_s\left(\frac{\varepsilon_u-\varepsilon'_{cr}}{f'_u-f'_{cr}}\right) & f'_u>f'_{cr}\\ -0.02E_s\left(\frac{\varepsilon_u-\varepsilon'_{cr}}{f'_u-f'_{cr}}\right) & f'_u\le f'_{cr}\end{cases} \tag{8}$$

The proposed steel model can capture the characteristics of the effective $\sigma-\varepsilon$ curve extracted from the FE analysis for the steel tube. An example is presented in Fig. 9(a) for the specimen R2 tested by Schneider (1998). The comparison indicates a very good agreement between the predicted effective steel $\sigma-\varepsilon$ curve from the proposed model and that obtained from the 3D FE analysis.

Material Model of Concrete

Characteristics of Effective Stress–Strain Curves for Concrete

For CFST columns, the development of passive confinement from the steel tubes can enhance the compressive strength and ductility of the infill concrete. The confinement factor ξ_c has been found to

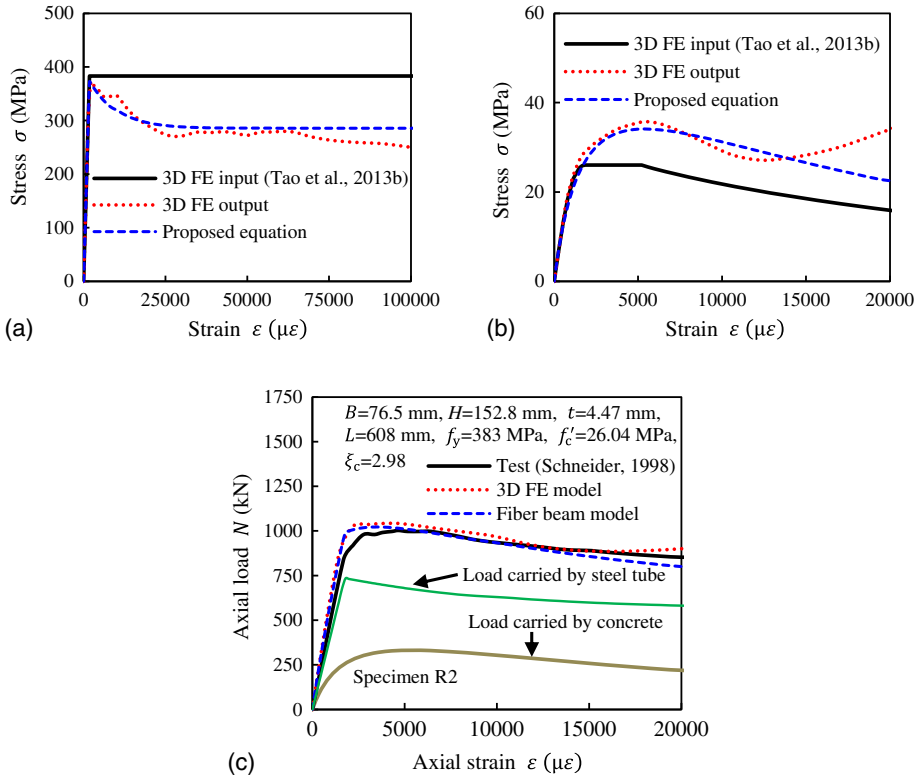

Fig. 9. Validation of steel and concrete material models: (a) comparison of steel models; (b) comparison of concrete models; and (c) comparison of predicted and measured $N-\varepsilon$ curves.

be a comprehensive parameter that reflects the intensity of concrete confinement (Han et al. 2014). Effective concrete $\sigma-\varepsilon$ curves for rectangular CFST columns with different ξ_c-values are extracted from the FE modeling and compared in Fig. 3(b). When the confinement is strong, there is an obvious enhancement in compressive strength and ductility of the infill concrete. But when ξ_c is small, the enhancement in strength and ductility of the infill concrete is limited because of the relatively weak confinement. Although concrete confinement in a rectangular tube is less effective than that in a circular tube, its influence on the effective concrete $\sigma-\varepsilon$ curve is not negligible for rectangular CFST columns, as can be seen in Fig. 3(b). Therefore, an effective concrete $\sigma-\varepsilon$ relationship is developed as follows to consider the confinement effect in rectangular CFST columns.

Proposed Effective Concrete Stress–Strain Relationship

Katwal et al. (2017) proposed Eq. (9) to represent the effective concrete $\sigma-\varepsilon$ relationship for circular CFST columns, where a total of five parameters are used in the concrete model, including the confined concrete strength (f'_{cc}) and corresponding ultimate strain (ε'_{cc}), residual stress (f_r), and coefficients a and b. It is worth noting that the coefficients a and b were used to determine the shape of the concrete $\sigma-\varepsilon$ curve, whereas the definitions of f'_{cc}, ε'_{cc}, and f_r are shown in Fig. 10

$$\sigma=\begin{cases}\dfrac{a\cdot X+b\cdot X^2}{1+(a-2)\cdot X+(b+1)\cdot X^2}\cdot f'_{cc} & X\le 1 \quad \text{or} \quad (X>1 \quad \text{and} \quad \sigma>f_r)\\ f_r & X>1 \quad \text{and} \quad \sigma\le f_r\end{cases} \tag{9}$$

where $X=\varepsilon/\varepsilon'_{cc}$.

It is found that Eq. (9) is still applicable for rectangular CFST columns, but those five parameters need to be recalibrated. Fig. 10 presents the schematic of two effective concrete $\sigma-\varepsilon$ curves with relatively high and low confinement, respectively. The input concrete curves used in 3D FE modeling are also depicted in the figure for comparison. When the confinement is weak, the difference between the concrete curve used in 3D FE modeling and the derived effective $\sigma-\varepsilon$ curve is relatively small. In contrast, the difference between them becomes significant when the confinement is strong.

Confined Concrete Strength f'_{cc} and Corresponding Ultimate Strain ε'_{cc}

The confined concrete strength f'_{cc} represents the enhancement of concrete strength because of the confinement provided by the steel tube. From the analysis of numerical data, it is found that

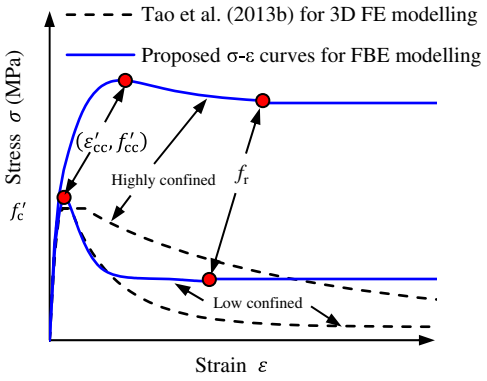

Fig. 10. Proposed concrete $\sigma - \varepsilon$ model for FBE modeling of rectangular CFST columns.

the strength enhancement is mainly dependent on ξ_c. The ratio of f_{cc}'/f_c' increases with increasing ξ_c. However, other parameters such as the D'/t ratio, f_c', f_y, and B/H are further introduced to improve the prediction accuracy of the proposed model. By performing regression analysis of the data generated from the 3D FE analysis, Eq. (10) is proposed to determine f_{cc}'

$$\frac{f_{cc}'}{f_c'} = \gamma_c \left[0.845 + \frac{f_y^{0.08}}{2(f_c')^{0.4}} + \frac{0.35(\xi_c)^{1.06}}{(D'/t)^{0.3}} \left(\frac{B}{H}\right)^{0.6} \right] \tag{10}$$

As mentioned earlier, size effect is prominent for rectangular CFST columns (Wu et al. 2018). Therefore, a strength correction factor γ_c is introduced into Eq. (10) to account for the size effect. Based on the trial-and-error method, the most suitable γ_c value for a specific specimen is suggested to achieve a good match (±1% error) between the measured ultimate strength and predicted one using FBE modeling. Accordingly, the obtained γ_c values are shown in triangles in Fig. 11 as a function of $D_c \left(= \sqrt{(B-2t)^2 + (H-2t)^2}\right)$. Because test errors have a direct impact in deriving γ_c, it is not surprising that scattered values are obtained for γ_c. Despite this, a clear trend can be found in Fig. 11 that γ_c decreases with increasing D_c. Sakino et al. (2004) proposed an equation for γ_c based on the test data of unconfined concrete. Through regression analysis of the suggested γ_c values in Fig. 11, Sakino et al.'s equation was refined and Eq. (11) is proposed to predict γ_c for core concrete confined by a rectangular steel tube. As can be seen in Fig. 11, the refined equation gives a slightly higher γ_c than the original equation proposed by Sakino et al. (2004). This reflects the fact that concrete confinement can reduce the size effect (Wang et al. 2017). Because there

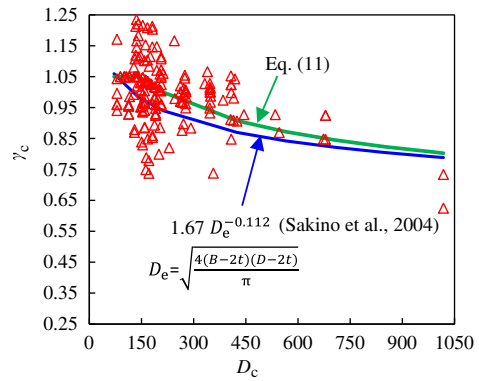

Fig. 11. Verification of proposed equation for γ_c.

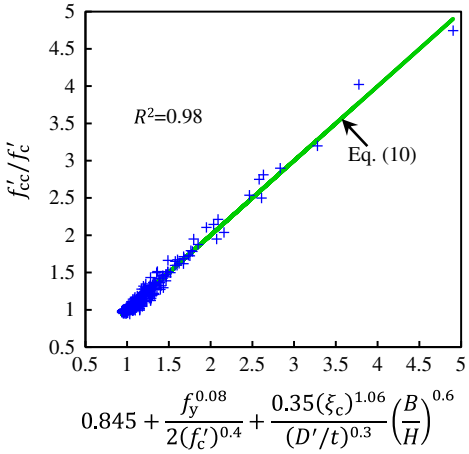

Fig. 12. Verification of proposed equation for f_{cc}'.

are no test data available for CFST columns with a D_c greater than 1,018 mm, it is not possible to revise Sakino et al.'s equation beyond this limit. Further research is required to propose γ_c beyond this limit

$$\gamma_c = \left(\frac{D_c}{212}\right)^{-0.14} \leq 1.05 \tag{11}$$

where $D_c = \sqrt{(B-2t)^2 + (H-2t)^2}$.

It is found that the introduction of the strength correction factor γ_c has greatly improved the prediction accuracy of large-size columns, which will be further discussed in the section describing the verification of FBE modeling for stub columns. Fig. 12 represents the prediction accuracy of Eq. (10), indicating that the predicted values of f_{cc}' have an excellent agreement with numerical data of 3D FE modeling ($R^2 = 0.98$). It should be noted that, in the comparison, γ_c was not introduced when calculating f_{cc}' as size effect was not considered in 3D FE modeling either.

The strain ε_{cc}' corresponding to f_{cc}' is found to be mainly affected by ξ_c and D'/t ratio. But the inclusion of the aspect ratio B/H and f_c' is found to further improve the prediction accuracy. So Eq. (12) is developed to predict ε_{cc}'. As shown in Fig. 13, a R^2 value of 0.97 represents a strong correlation between the predictions and numerical results

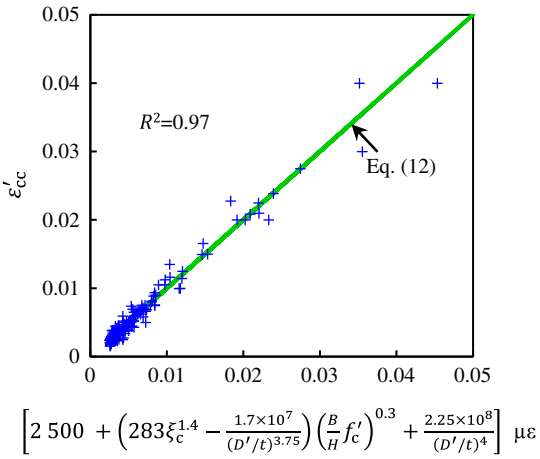

Fig. 13. Verification of proposed equation for ε_{cc}'.

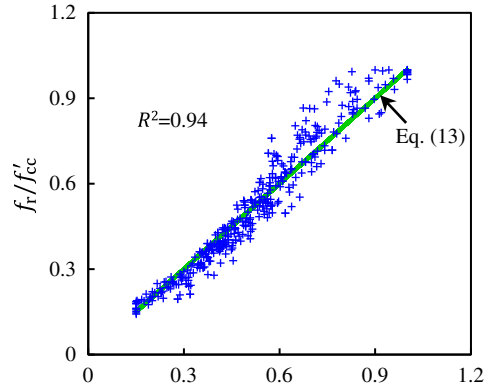

$$0.96\xi_c^{0.1} + \frac{9.7}{(D'/t)^{1.5}} + 0.09\sqrt{\frac{f_y}{f'_c}\frac{B}{H}} - 0.7$$

Fig. 14. Verification of proposed equation for f_r.

$$\varepsilon'_{cc} = 2500 + \left(283\xi_c^{1.4} - \frac{1.7\times10^7}{(D'/t)^{3.75}}\right)\left(\frac{B}{H}f'_c\right)^{0.3} + \frac{2.25\times10^8}{(D'/t)^4}(\mu\varepsilon) \tag{12}$$

Residual Concrete Strength f_r

The definition of residual concrete strength (f_r) is important to analyze columns with large deformation. The data obtained from the FE analysis indicate that f_r is mainly dependent on ξ_c. The ratio of f_r/f'_{cc} increases with increasing ξ_c. When ξ_c is very large, f_r is close to f'_{cc} because of strong confinement, as shown in Fig. 3(b). To improve the prediction accuracy, D'/t, f_y/f'_c and B/H are also included in the regression analysis in proposing Eq. (13) to predict f_r. A reasonably good agreement ($R^2 = 0.94$) is obtained between the proposed equation and numerical results, as shown in Fig. 14

$$\frac{f_r}{f'_{cc}} = 0.96\xi_c^{0.1} + \frac{9.7}{(D'/t)^{1.5}} + 0.09\sqrt{\frac{f_y}{f'_c}\frac{B}{H}} - 0.7 \le 1 \text{ and } \ge 0.15 \tag{13}$$

Coefficients a and b

Coefficient a controls the shape of the ascending part of the $\sigma - \varepsilon$ curve. Eq. (14) was proposed by Katwal et al. (2017) for circular CFST columns, which was a modified equation originally proposed by Samani and Attard (2012) for concrete under active confinement. It is found that Eq. (14) can still be used for rectangular CFST columns by recalibrating α_1 as presented in Eq. (15)

$$a = \alpha_1 \frac{E_c\varepsilon'_{cc}}{f'_{cc}} \tag{14}$$

where E_c is the modulus of elasticity of unconfined concrete, taking as $4{,}700\sqrt{f'_c}$ MPa according to ACI 318-19 (ACI 2019). The unit for f'_c is MPa

$$\alpha_1 = 1 + 0.2 \cdot \xi_c^{(0.05+0.2/\xi_c)} \tag{15}$$

Coefficient b mainly controls the slope of the descending branch. For circular CFST columns, the value of b varies between −0.75 and 2 (Katwal et al. 2017). However, for rectangular CFST columns, it is found that b is generally negative and in the range from −0.75 to 0. Accordingly, Eq. (16) was developed to determine b for rectangular columns based on regression analysis

$$b = 0.15 - e^{(-1.4\xi_c^{0.8})} - 0.012\left(\frac{f'_c D'}{t}\right)^{0.3}\left(\frac{H}{B}\right)^2 \ge -0.75 \le 0 \tag{16}$$

The developed concrete model has well captured the characteristics of the effective $\sigma - \varepsilon$ curves of concrete obtained from 3D FE modeling, as shown in Fig. 9(b). Accordingly, the predicted axial load–axial strain curve from the simplified simulation [Fig. 9(c)] matches well with the predicted curve from the 3D FE modeling and experimental curve of Specimen R2 tested by Schneider (1998). More comparisons are given in the following section to verify the simplified FBE modeling.

Verification of FBE Modeling for Stub Columns

The proposed simplified FBE modeling for rectangular CFST stub columns is further verified by test results of 183 test specimens. These test data are collected from 24 different sources. Most of the experimental data have been previously used by Tao et al. (2013b) in developing 3D FE models for CFST stub columns. Recently reported test data of large-size columns (Chen et al. 2012; Wu et al. 2018), columns with ultrahigh strength concrete (Xiong et al. 2017), and very stocky columns (Yan et al. 2019) are further added to the database. As presented in Table 1, the collected experimental data cover a wide range of parameters: f_y = 194–835 MPa, f'_c = 13–159 MPa, B = 60–750 mm, B/t = 5–150, and H/B = 1–2.

Fig. 15 compares the predicted ultimate strengths (N_{uc}) from the simplified simulation with predictions from the 3D FE modeling (N_{uFE}) and measured ultimate strengths (N_{ue}). In both the simplified simulation and 3D FE modeling, the size effect was not considered.

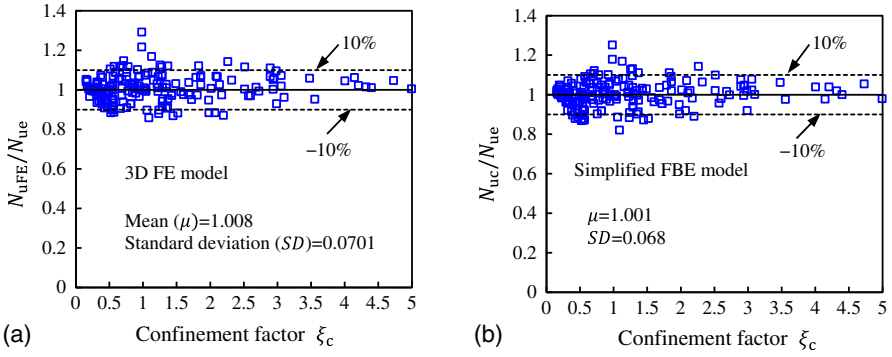

Fig. 15. Comparison of N_{ue} with N_{uFE} and N_{uc} with respect to ξ_c for CFST stub columns without considering size effect: (a) comparison between N_{uFE} and N_{ue}; and (b) comparison between N_{uc} and N_{ue}.

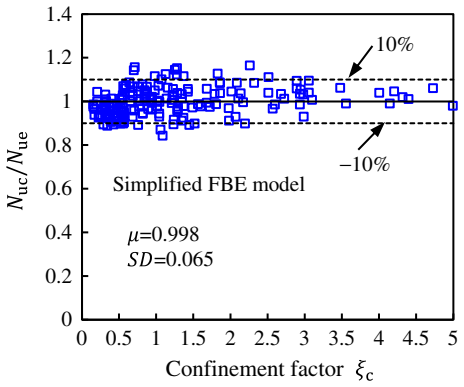

Fig. 16. Comparison of N_{ue} with N_{uc} with respect to ξ_c for CFST stub columns considering size effect.

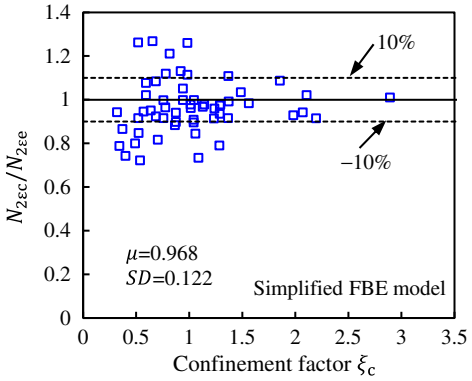

Fig. 17. Prediction accuracy of $N_{2\varepsilon c}/N_{2\varepsilon e}$ with respect to ξ_c.

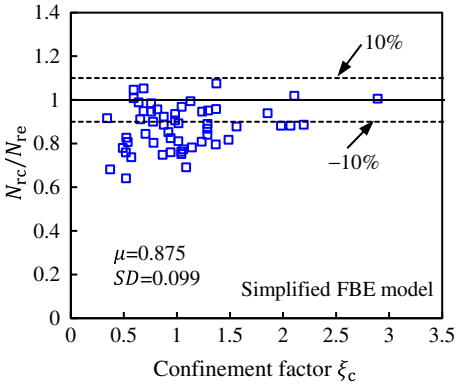

Fig. 18. Prediction accuracy of N_{rc}/N_{re} with respect to ξ_c.

The definition of the ultimate strength follows that in Tao et al. (2013b) and Katwal et al. (2017). It is taken as the peak load if the $N-\varepsilon$ curve has a descending branch and the peak strain corresponding to the peak load is less than or equal to 1%. Otherwise, the ultimate strength is defined as the load corresponding to 1% strain. The mean (μ) and standard deviation (SD) for the N_{uFE}/N_{ue} ratio are 1.008 and 0.071, respectively. Meanwhile, the corresponding μ and SD for the N_{uc}/N_{ue} ratio are 1.001 and 0.068, respectively. In general, good predictions of the ultimate strength have been obtained from both the 3D FE and simplified simulations. However, a large scatter is found in the predictions from both the 3D FE and simplified simulations. The scatter is particularly obvious for those large-size specimens. After the size effect is considered in the FBE modeling, improvement in prediction accuracy of the ultimate strength can be seen in Fig. 16. The corresponding μ and SD for the N_{uc}/N_{ue} ratio are 0.998 and 0.065, respectively. Due to the limited number of large-size columns, the improvement in the values of μ and SD is not very significant after considering the size effect. But less scatter in the prediction accuracy of N_{uc} can be easily found by comparing Fig. 16 with Fig. 15(b).

To further verify the prediction accuracy of the postpeak stage, the predicted load at $2\varepsilon_{cc}$ and the residual strength corresponding to an axial strain of 0.015 are compared with experimental results of 54 specimens tested in a displacement control mode. These test data are from eight sources (Tomii et al. 1977; Uy 2000; Yamamoto et al. 2000; Huang et al. 2002; Liu 2005; Chen et al. 2012; Xiong et al. 2017; Wu et al. 2018). It should be noted that the strain softening response might not be reliably captured through testing in a load control manner. Therefore, the relevant test data are discarded in this comparison. The μ and SD of the ratio of the predicted load ($N_{2\varepsilon c}$) at $2\varepsilon_{cc}$ to the measured load ($N_{2\varepsilon e}$) at $2\varepsilon_{cc}$ are 0.968 and 0.122, respectively (Fig. 17). It seems that reasonable accuracy has been obtained in predicting the load at $2\varepsilon_{cc}$. On the other hand, the μ and SD of the ratio of the predicted residual strength (N_{rc}) to the measured residual strength (N_{re}) are 0.875 and 0.099, respectively (Fig. 18). As can be seen, the prediction accuracy for the residual strength is also reasonable, but generally on the safe side.

To compare the predicted load–deformation curves with test curves, Katwal et al. (2017) divided circular CFST columns into different groups based on the steel and concrete strengths. According to the compressive strength, concrete was classified into three categories: normal strength concrete (NSC: $f'_c \le 60$ MPa), high strength concrete (HSC: 60 MPa $< f'_c \le 120$ MPa), and ultrahigh strength concrete (UHSC: $f'_c > 120$ MPa). Similarly, steel was classified into two categories based on the yield stress: normal strength steel (NSS: $f_y < 460$ MPa) and high strength steel (HSS: $f_y \ge 460$ MPa). This classification method is also applied to rectangular CFST columns in this study.

Fig. 19 compares the predicted $N-\varepsilon$ curves with measured curves of Specimens R4 (Schneider 1998) and sczs2-2-4 (Han et al. 2001) made with NSC and NSS. It can be observed that the predicted curves agree very well with the measured curves and those predicted from the 3D FE modeling. Compared with the 3D FE modeling, the simplified FBE modeling can predict the initial stiffness, ultimate strength, and residual strength very well with very low computational cost. Based on the FBE simulation, the loads resisted by the steel tube and infill concrete are also presented in Fig. 19 for each specimen. The ξ_c-value for Specimen R4 is 2.57, which is higher than the corresponding value of 1.34 for sczs2-2-4. Therefore, it is expected that the concrete in R4 is better confined than that in sczs2-2-4. This explains the better ductility of concrete in R4, although the relative strength contribution from the concrete for this specimen is much lower than that in sczs2-2-4. The prediction accuracy for columns with NSC and NSS can also be observed in Fig. 9, where Specimen R2 tested by Schneider (1998) was selected for comparison.

To demonstrate the prediction accuracy of the proposed FBE model for specimens with HSC, two specimens including C3 tested by Liu et al. (2003) and A5-1 tested by Liu and Gho (2005) are selected, where their f'_c-values are 60.8 and 106 MPa, respectively. For the two specimens, the strength contribution from the HSC is more than that of the steel tube. Therefore, the specimens exhibit relatively low ductility. In this paper, ductility refers to the ability of a column to deform inelastically without significant deterioration in

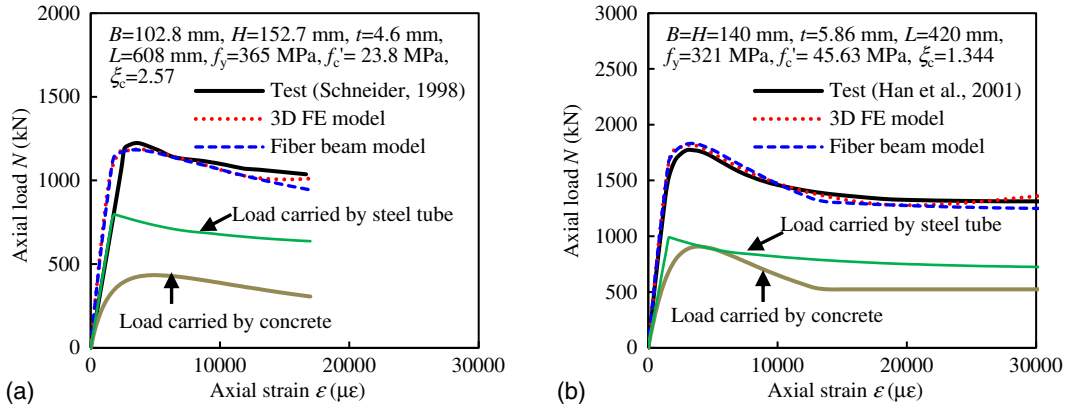

Fig. 19. Comparison of predicted and measured $N-\varepsilon$ curves for stub columns with normal materials: (a) Specimen R4; and (b) Specimen sczs2-2-4.

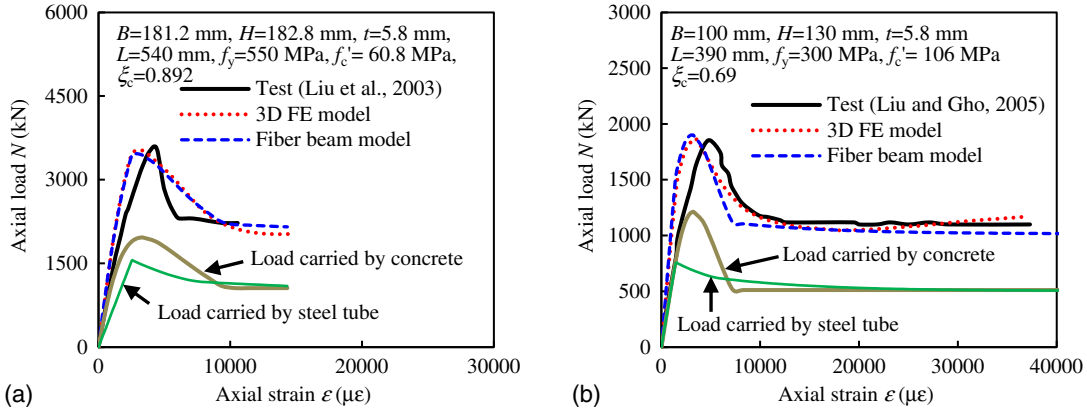

Fig. 20. Comparison of predicted and measured $N-\varepsilon$ curves for stub columns with HSC: (a) Specimen C3; and (b) Specimen A5-1.

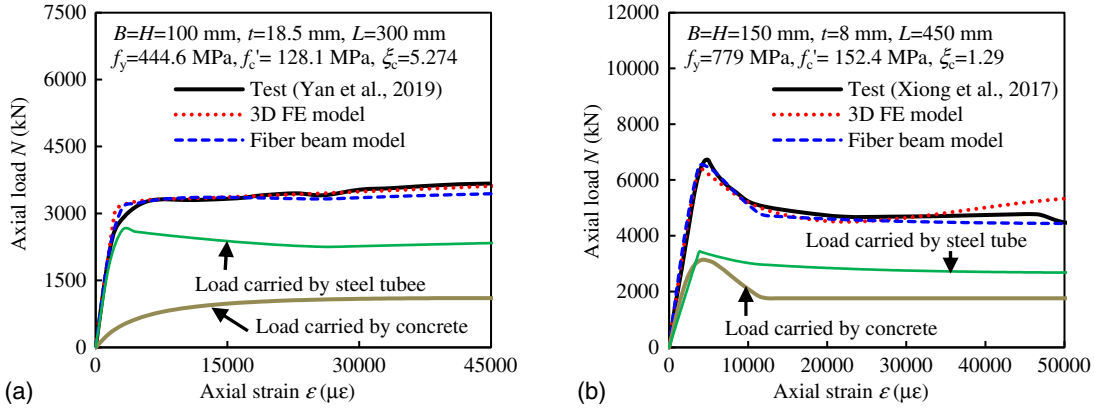

Fig. 21. Comparison of predicted and measured $N-\varepsilon$ curves for stub columns with UHSC: (a) Specimen S16-18-140; and (b) Specimen S2.

strength. The comparisons shown in Fig. 20 demonstrate the very good predictions by FBE modeling for rectangular CFST columns with HSC.

Specimen S16-18-140 ($f_c' = 128.1$ MPa) tested by Yan et al. (2019) and Specimen S2 ($f_c' = 152.4$ MPa) tested by Xiong et al. (2017) are selected to demonstrate the prediction accuracy of the FBE model for rectangular CFST columns with UHSC. It should be noted that HSS was also used in fabricating S2. As can be seen in Fig. 21, FBE modeling has captured well the $N-\varepsilon$ curves of both Specimens S16-18-140 and S2. As very thick steel tubes are used in both specimens, the steel tube contributes more to the strength of each composite column than the concrete. Therefore, both specimens exhibit very good ductility.

To demonstrate the prediction accuracy for rectangular CFST columns with HSS, two specimens were selected, including R1-1 ($f_y = 495$ MPa) tested by Liu (2005) and CR8-A-8 ($f_y = 835$ MPa)

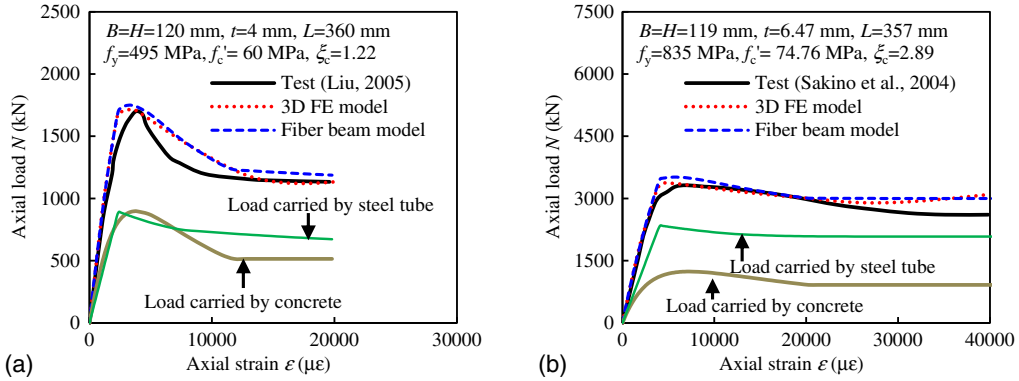

Fig. 22. Comparison of predicted and measured $N-\varepsilon$ curves for stub columns with HSS: (a) Specimen R1-1; and (b) Specimen CR8-A-8.

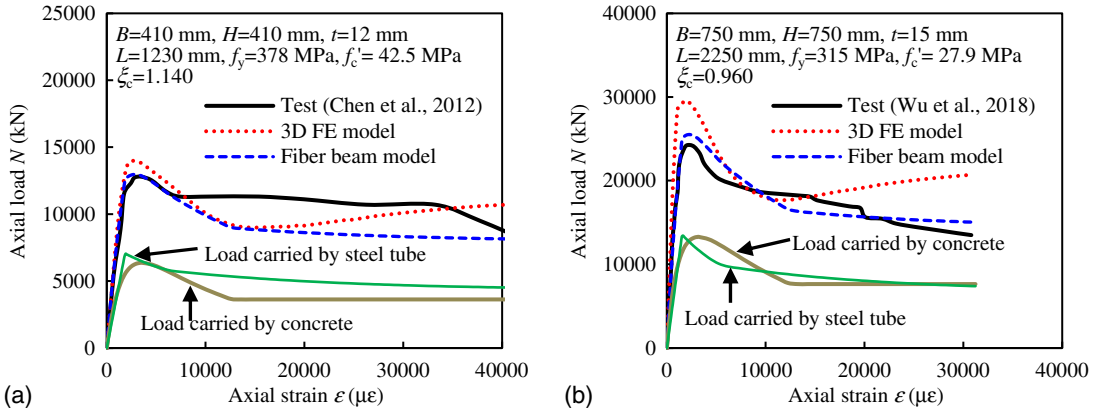

Fig. 23. Comparison of predicted and measured $N-\varepsilon$ curves for large-size columns: (a) Specimen AA-32; and (b) Specimen A750-b.

tested by Sakino et al. (2004). As shown in Fig. 22, the FBE model can predict the $N-\varepsilon$ curves for specimens in this category as well.

Finally, the prediction accuracy of the FBE model is demonstrated for large-size columns ($B \geq 300$ mm). Figs. 23(a and b) show the prediction accuracy for Specimens AA-32 ($B = 410$ mm) and A750-b ($B = 750$ mm) tested by Chen et al. (2012) and Wu et al. (2018), respectively. The predicted peak loads from the 3D FE modeling are 9% and 21% higher than the measured peak loads for AA-32 and A750-b, respectively. This is because the 3D FE modeling did not consider the size effect. Therefore, it can give unsafe predictions for large-size columns. After considering the size effect, the FBE modeling provides better predictions of $N-\varepsilon$ curves for large-size columns (Fig. 23).

FBE Modeling of Slender Columns

If the strain gradient effect is ignored, the uniaxial effective $\sigma-\varepsilon$ models of steel and concrete proposed in the previous section may be further used in simulating rectangular CFST slender columns. A similar approach has been adopted by Han et al. (2001) and Lai and Varma (2016). In this study, slender columns refer to those with $L/B > 5$ and subjected to axial compression, where L is the effective length of a column. In previous tests on slender columns, pinned boundary conditions have been commonly used. To compare with test results, such boundary conditions are defined for rectangular CFST slender columns in the FBE modeling. For slender columns, tensile stresses may develop in some part of the cross section due to the second-order effect. Therefore, for steel and concrete in tension, the corresponding $\sigma-\varepsilon$ models presented by Tao et al. (2013a) and Katwal et al. (2018), respectively, are adopted.

In simulating slender columns, it is very important to introduce initial imperfections to capture the possible strength reduction due to the second-order effect. In the current study, this is achieved by scaling the first eigenvalue buckling mode shape. Different amplitudes of initial imperfections have been used by previous researchers, such as $L/5{,}000$, $L/1{,}500$, $L/1{,}000$, and $L/500$. The most widely used amplitude of initial imperfections in previous numerical analysis of slender CFST columns is $L/1{,}000$ (Patel et al. 2012; Tao et al. 2016). Therefore, this amplitude is also adopted in this study. Nonetheless, a sensitivity analysis is conducted to study the influence of initial imperfection amplitude on the axial load versus midheight deflection ($N-u_m$) curve. The square specimen scp2-1-1 tested by Han et al. (2001) was selected as an example, which has a cross-sectional width of 200 mm and an effective length of 2,600 mm. Three different imperfection amplitudes ($L/5{,}000$, $L/1{,}000$, and $L/500$) are tried and the different $N-u_m$ curves predicted from the FBE modeling are compared in Fig. 24(a). As can be seen, the initial imperfection amplitude (Δ) has a significant influence on the predicted stiffness and peak load for the slender column. When Δ is taken as $L/5{,}000$, the stiffness and peak load are significantly overestimated. On the other hand, the stiffness and peak load are slightly underestimated when Δ is taken as $L/500$. For this specimen, a value of $L/1{,}000$ is the most suitable amplitude for predicting the $N-u_m$ curve.

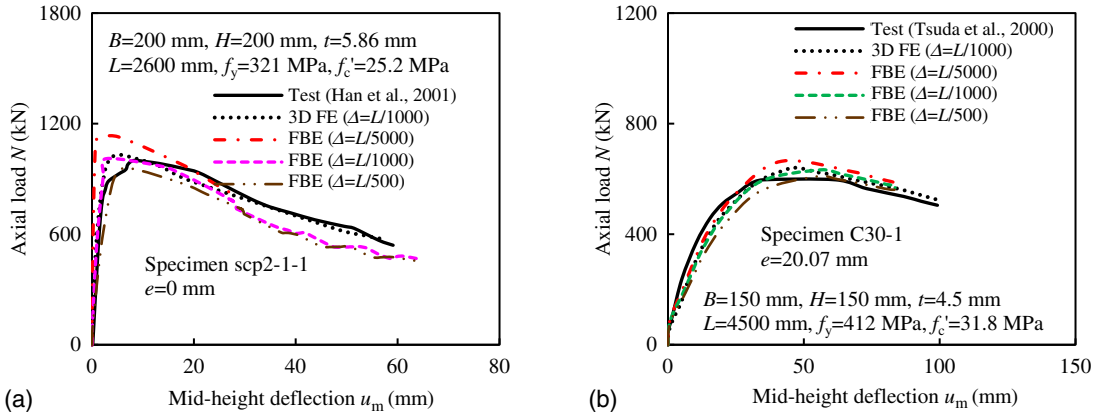

Fig. 24. Sensitivity analysis on the initial imperfection amplitude: (a) slender column; and (b) beam-column.

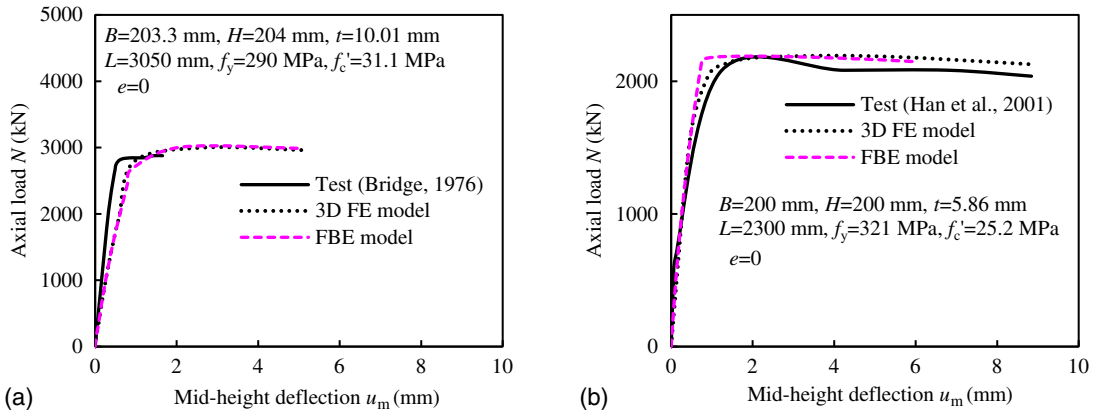

Fig. 25. Comparison of predicted and measured $N - u_m$ curves of slender columns: (a) Specimen SHC-2; and (b) Specimen scp2-3-1.

In simulating slender columns and beam-columns, it was found that using the Dynamic Implicit solver available in ABAQUS makes it much easier to achieve convergence than using the static method. Therefore, the Dynamic Implicit solver was used for both slender columns and beam-columns in either FBE or 3D FE simulation. Because the loading was static, it was applied using a quasi-static option in ABAQUS to minimize the dynamic effects. Thus, the kinetic energy of the FBE model was kept at less than 2% of the internal energy in all cases, ensuring that the results were not adversely affected by the selection of the Dynamic Implicit analysis.

In addition to Specimen scp2-1-1 tested by Han et al. (2001), two other specimens, including SHC-2 tested by Bridge (1976) and scp2-3-1 tested by Han et al. (2001), are selected to further verify the prediction accuracy of the FBE model for slender rectangular CFST columns. Meanwhile, 3D FE models have also been built for those columns by adopting the same material models, element types, and interaction between the steel and concrete as suggested by Tao et al. (2013b) for rectangular CFST stub columns. However, initial imperfections with an amplitude of $L/1{,}000$ were introduced into the 3D FE models to simulate slender columns following the same procedure adopted in FBE modeling. Figs. 24 and 25 compare the predicted $N - u_m$ curves from the FBE modeling with the experimental curves and predicted curves from 3D FE modeling. It can be seen that the FBE modeling results ($\Delta = L/1{,}000$) correlate well with the test results as well as the 3D FE modeling results. It seems that reasonable accuracy can be achieved when the uniaxial effective $\sigma - \varepsilon$ models of steel and concrete developed in this study are used in simulating rectangular CFST slender columns. However, further research can be conducted to consider the influence of the strain gradient effect on the concrete $\sigma - \varepsilon$ model. This might further improve the prediction accuracy, especially for CFST columns with strong confinement (Lin et al. 2020).

FBE Modeling of Beam-Columns

The developed FBE model is further utilized to check its ability to simulate rectangular CFST beam-columns. In this study, beam-columns refer to members subjected to eccentric compression. To apply eccentric loading in the FBE model, rigid beams perpendicular to the column axis are added in connection with the top and bottom ends of the beam elements representing the column. Then concentrated loads are applied to the rigid beams with the required load eccentricity. Other procedures regarding the development of the FBE model for beam-columns are the same as those described in the earlier section for slender columns. Three-dimensional FE models are also developed to simulate beam-columns. The 3D FE model of a beam-column is quite similar to that of a slender column under axial compression, except for the introduction of load eccentricity to the beam-column at the ends.

For beam-columns, the introduction of initial imperfections normally only has limited influence on the member performance provided the load eccentricity is large enough. This can be seen from the sensitivity analysis shown in Fig. 24(b) for Specimen C30-1

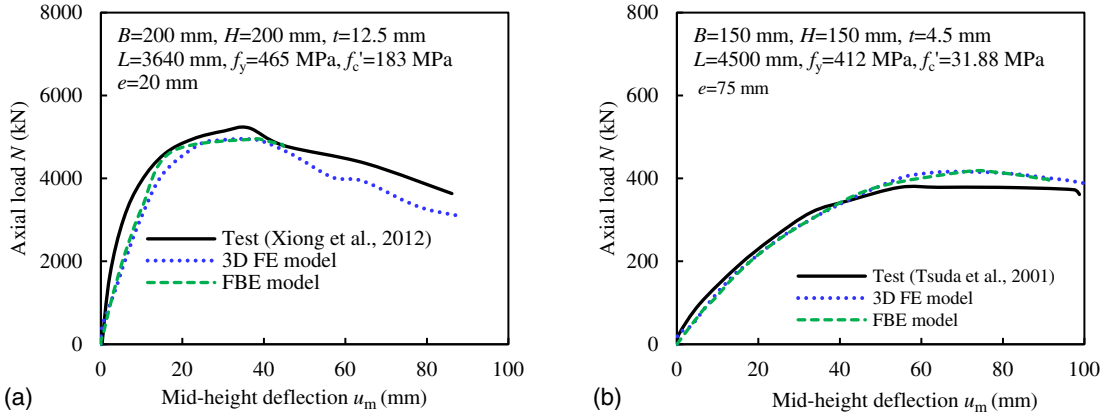

Fig. 26. Comparison between predicted and measured $N - u_m$ curves of beam-columns: (a) Specimen SS-1; and (b) Specimen C30-3.

tested by Tsuda et al. (2000). This specimen has a cross-sectional width of 150 mm, an effective length of 4,500 mm, and a load eccentricity of 20.07 mm. It seems that the adoption of an initial imperfection amplitude of $L/1{,}000$ (= 4.5 mm) leads to the best prediction of the $N - u_m$ curve. Therefore, initial imperfections are still considered in simulating beam-columns by adopting an amplitude of $L/1{,}000$.

To further verify the prediction accuracy of FBE modeling for beam-columns, Specimen SS-1 tested by Xiong (2012) and Specimen C30-2 tested by Tsuda et al. (2000) are selected for comparison. As can be seen in Fig. 26, the $N - u_m$ curves obtained from FBE modeling are in good agreement with the measured curves and those obtained from the 3D FE modeling. Although the FBE model underestimates the initial stiffness of SS-1, a similar tendency is found for the 3D FE model. It seems that the proposed effective $\sigma - \varepsilon$ models of steel and concrete can also be adopted in simulating rectangular CFST beam-columns.

Concluding Remarks

In simplified simulation of CFST columns, the simulation accuracy largely depends on the input steel and concrete material models, which should implicitly consider the material nonlinearity and interaction between the steel and concrete components. In this paper, uniaxial effective steel and concrete material models have been developed for rectangular CFST columns based on rigorous analysis of data generated from 3D FE modeling of axially loaded stub columns. The proposed effective material model of steel has implicitly considered the interaction between the steel and concrete as well as yielding and possible local buckling of the steel tube. Similarly, the proposed effective stress–strain model of concrete has implicitly considered the enhancement in strength and ductility due to confinement provided by the steel tube. Meanwhile, a strength correction factor has been introduced into the concrete model to consider the size effect. The proposed steel and concrete material models are valid within the following parameter ranges: concrete compressive strength ($f'_c = 20$–200 MPa), yield stress of steel ($f_y = 200$–960 MPa), cross-sectional aspect ratio ($H/B = 1$–2), and width-to-thickness ratio ($B/t = 5$–150).

The effective steel and concrete material models have been successfully incorporated into FBE modeling of slender columns and beam-columns. The obtained load–deformation curves from FBE modeling are in good agreement with the measured curves and those obtained from 3D FE modeling. As the FBE model is more computationally efficient than the 3D FE model, the former has the potential to be widely used for analyzing CFST columns due to its accuracy and simplicity. Further research can be conducted to check the suitability of adopting the proposed material models to analyze structural frames with rectangular CFST columns.

Data Availability Statement

Some or all data, models, or code that support the findings of this study are available from the corresponding author upon reasonable request.

Acknowledgments

The authors are grateful for the financial support from the Australian Research Council Discovery Grant No. DP170100001.

Notation

The following symbols are used in this paper:

A_c = cross-sectional area of core concrete;
A_s = cross-sectional area of a steel tube;
a = parameter controlling ascending part of the concrete model;
B = overall cross-sectional width;
b = parameter controlling descending part of the concrete model;
D_c = diagonal distance between outer corners of core concrete;
D' = diagonal distance between outer corners of the cross section of a rectangular steel tube;
E_c = Young's modulus of concrete;
E_s = Young's modulus of steel;
f'_c = concrete cylinder compressive strength;
f'_{cc} = confined concrete strength;
f'_{cr} = critical steel stress;
f_r = residual stress of concrete;
f'_u = effective stress corresponding to the ultimate strain of steel;
f_y = yield stress of steel;
f'_y = first peak stress of steel;
H = overall cross-sectional depth;
L = length of column;

N = axial load;
N_e = measured residual strength;
N_r = predicted residual strength;
N_{uc} = predicted ultimate strength based on the FBE model;
N_{ue} = measured ultimate strength;
N_{uFE} = predicted ultimate strength based on the FE model;
$N_{2\varepsilon c}$ = predicted load at $2\varepsilon_{cc}$;
$N_{2\varepsilon e}$ = measured load at $2\varepsilon_{cc}$;
P_0 = simple summation of strength of the steel section and core concrete;
p = strain softening/hardening exponent beyond the critical point for steel;
R^2 = coefficient of determination;
SD = standard deviation;
t = thickness of a steel tube;
u_m = midspan deflection;
α_1 = coefficient used in determining a;
γ_c = strength correction factor;
Δ = imperfection amplitude;
ε = strain;
ε'_{cc} = strain corresponding to f'_{cc} of core concrete;
ε_{c0} = peak strain of unconfined concrete;
ε'_{cr} = critical steel strain;
ε_u = strain corresponding to tensile strength of steel;
ε_y = yield strain of steel;
ε'_y = strain corresponding to the first peak stress of steel f'_y;
μ = mean value;
ξ_c = confinement factor;
σ = stress; and
ψ = strain softening exponent.

References

ACI (American Concrete Institute). 2019. *Building code requirements for structural concrete and commentary.* ACI 318-19. Farmington Hills, MI: ACI.

Bridge, R. Q. 1976. *Concrete filled steel tubular columns*. Rep. No. R283. Sydney, Australia: Univ. of Sydney.

Chen C. C., J. W. Ko, G. L. Huang, and Y. M. Chang. 2012. "Local buckling and concrete confinement of concrete-filled box columns under axial load." *J. Constr. Steel Res.* 78 (Nov): 8–21. https://doi.org/10.1016/j.jcsr.2012.06.006.

De Nicolo, B., L. Pani, and E. Pozzo. 1994. "Strain of concrete at peak compressive stress for a wide range of compressive strengths." *Mater. Struct.* 27 (4): 206–210. https://doi.org/10.1007/BF02473034.

Han, L. H. 2002. "Tests on stub columns of concrete-filled RHS sections." *J. Constr. Steel Res.* 58 (3): 353–372. https://doi.org/10.1016/S0143-974X(01)00059-1.

Han, L. H., W. Li, and R. Bjorhovde. 2014. "Developments and advanced applications of concrete-filled steel tubular (CFST) structures: Members." *J. Constr. Steel Res.* 100 (Sep): 211–228. https://doi.org/10.1016/j.jcsr.2014.04.016.

Han, L. H., and G. H. Yao. 2004. "Experimental behavior of thin-walled hollow structural steel (HSS) columns filled with self-consolidating concrete (SCC)." *Thin-Walled Struct.* 42 (9): 1357–1377. https://doi.org/10.1016/j.tws.2004.03.016.

Han, L. H., G. H. Yao, and X. L. Zhao. 2005. "Tests and calculations for hollow structural steel (HSS) stub columns filled with self-consolidating concrete (SCC)." *J. Constr. Steel Res.* 61 (9): 1241–1269. https://doi.org/10.1016/j.jcsr.2005.01.004.

Han, L. H., X. L. Zhao, and Z. Tao. 2001. "Tests and mechanics model for concrete-filled SHS stub columns, columns and beam-columns." *Steel Compos. Struct.* 1 (1): 51–74. https://doi.org/10.12989/scs.2001.1.1.051.

Huang, C. S., Y. K. Yeh, G. Y. Liu, H. T. Hu, K. C. Tsai, Y. T. Weng, S. H. Wang, and M. H. Wu. 2002. "Axial load behavior of stiffened concrete-filled steel columns." *J. Struct. Eng.* 128 (9): 12221230. https://doi.org/10.1061/(ASCE)0733-9445(2002)128:9(1222).

Katwal, U., Z. Tao, and M. K. Hassan. 2018. "Finite element modelling of steel-concrete composite beams with profiled steel sheeting." *J. Constr. Steel Res.* 146 (Jul): 1–15. https://doi.org/10.1016/j.jcsr.2018.03.011.

Katwal, U., Z. Tao, M. K. Hassan, and W. D. Wang. 2017. "Simplified numerical modeling of axially loaded circular concrete-filled steel stub columns." *J. Struct. Eng.* 143 (12): 04017169. https://doi.org/10.1061/(ASCE)ST.1943-541X.0001897.

Lai, Z., and A. H. Varma. 2016. "Effective stress-strain relationships for analysis of noncompact and slender filled composite (CFT) members." *Eng. Struct.* 124 (Oct): 457–472. https://doi.org/10.1016/j.engstruct.2016.06.028.

Lam, D., and C. A. Williams. 2004. "Experimental study on concrete filled square hollow sections." *Steel Compos. Struct.* 4 (2): 95–112. https://doi.org/10.12989/scs.2004.4.2.095.

Liang, Q. Q., B. Uy, and J. Y. R. Liew. 2006. "Nonlinear analysis of concrete-filled thin-walled steel box columns with local buckling effects." *J. Constr. Steel Res.* 62 (6): 581–591. https://doi.org/10.1016/j.jcsr.2005.09.007.

Lin, G., J. J. Zeng, J. G. Teng, and L. J. Li. 2020. "Behavior of large-scale FRP-confined rectangular RC columns under eccentric compression." *Eng. Struct.* 216 (Aug): 110759. https://doi.org/10.1016/j.engstruct.2020.110759.

Lin, S., and Y. G. Zhao. 2019. "Numerical study of the behaviors of axially loaded large-diameter CFT stub columns." *J. Constr. Steel Res.* 160 (Sep): 54–66. https://doi.org/10.1016/j.jcsr.2019.05.020.

Liu, D. 2005. "Tests on high-strength rectangular concrete-filled steel hollow section stub columns." *J. Constr. Steel Res.* 61 (7): 602–901. https://doi.org/10.1016/j.jcsr.2005.01.001.

Liu, D., and W. M. Gho. 2005. "Axial load behavior of high-strength rectangular concrete-filled steel tubular columns." *Thin-Walled Struct.* 43 (8): 1131–1142. https://doi.org/10.1016/j.tws.2005.03.007.

Liu, D., W. M. Gho, and J. Yuan. 2003. "Ultimate capacity of high-strength rectangular concrete-filled steel hollow section stub columns." *J. Constr. Steel Res.* 59 (12): 14991515. https://doi.org/10.1016/S0143-974X(03)00106-8.

Lu, Y., and D. Kennedy. 1992. *The flexural behavior of concrete-filled hollow structural sections*. Rep. No. 178. Edmonton, AB: Univ. of Alberta.

O'Shea, M. D., and R. Q. Bridge. 1997. *Behavior of thin-walled box sections with lateral restraint*. Rep. No. R739. Sydney, Australia: Univ. of Sydney.

Patel, I. P., Q. Q. Liang, and M. N. S. Hadi. 2012. "High strength thin-walled rectangular concrete-filled steel tubular slender beam-columns. Part II: Behavior." *J. Constr. Steel Res.* 70 (Mar): 368–376. https://doi.org/10.1016/j.jcsr.2011.10.021.

Sakino, K., H. Nakahara, S. Morino, and I. Nishiyama. 2004. "Behavior of centrally loaded concrete-filled steel-tube short columns." *J. Struct. Eng.* 130 (2): 180–188. https://doi.org/10.1061/(ASCE)0733-9445(2004)130:2(180).

Samani, A. K., and M. M. Attard. 2012. "A stress–strain model for uniaxial and confined concrete under compression." *Eng. Struct.* 41 (Aug): 335–349. https://doi.org/10.1016/j.engstruct.2012.03.027.

Schneider, S. P. 1998. "Axially loaded concrete-filled steel tubes." *J. Struct. Eng.* 124 (10): 1125–1138. https://doi.org/10.1061/(ASCE)0733-9445(1998)124:10(1125).

Tao, Z., M. Ghannam, T. Y. Song, and L. H. Han. 2016. "Experimental and numerical investigation of concrete-filled stainless steel columns exposed to fire." *J. Constr. Steel Res.* 118 (Mar): 120–134. https://doi.org/10.1016/j.jcsr.2015.11.003.

Tao, Z., L. H. Han, and D. Y. Wang. 2008. "Strength and ductility of stiffened thin-walled hollow steel structural stub columns filled with concrete." *Thin-Walled Struct.* 46 (10): 11131128. https://doi.org/10.1016/j.tws.2008.01.007.

Tao, Z., L. H. Han, and Z. B. Wang. 2005. "Experimental behavior of stiffened concrete-filled thin-walled hollow steel structural (HSS) stub columns." *J. Constr. Steel Res.* 61 (7): 962–983. https://doi.org/10.1016/j.jcsr.2004.12.003.

Tao, Z., B. Uy, L. H. Han, and Z. B. Wang. 2009. "Analysis and design of concrete-filled stiffened thin-walled steel tubular columns under axial compression." *Thin-Walled Struct.* 47 (12): 1544–1556. https://doi.org/10.1016/j.tws.2009.05.006.

Tao, Z., X. Q. Wang, and B. Uy. 2013a. "Stress–strain curves of structural and reinforcing steels after exposure to elevated temperatures." *J. Mat. Civ. Eng.* 25 (9): 1306–1316. https://doi.org/10.1061/(ASCE)MT.1943-5533.0000676.

Tao, Z., Z. B. Wang, and Q. Yu. 2013b. "Finite element modeling of concrete-filled steel stub columns under axial compression." *J. Constr. Steel Res.* 89 (Oct): 121–131. https://doi.org/10.1016/j.jcsr.2013.07.001.

Thai, H. T., B. Uy, M. Khan, Z. Tao, and F. Mashiri. 2014. "Numerical modelling of concrete-filled steel box columns incorporating high strength materials." *J. Constr. Steel Res.* 102 (Nov): 256265. https://doi.org/10.1016/j.jcsr.2014.07.014.

Thai, H. T., B. Uy, and M. A. Khan. 2015. "A modified stress-strain model accounting for the local buckling of thin-walled stub columns under axial compression." *J. Constr. Steel Res.* 111 (Aug): 57–69. https://doi.org/10.1016/j.jcsr.2015.04.002.

Tomii, M., K. Yoshimura, and Y. Morishita. 1977. "Experimental studies on concrete filled steel tubular stub columns under concentric loading." In *Proc., Int. Colloquium on Stability of Struct. under Static and Dynamic Loads*, 718–741. Reston, VA: ASCE.

Tsuda, K., C. Matsui, and E. Mino. 2000. "Strength and behavior of slender concrete filled steel tubular columns." In *Proc., 12th World Conf. on Earthquake Engineering*. Wellington, New Zealand: New Zealand Society for Earthquake Engineering.

Uy, B. 2000. "Strength of concrete filled steel box columns incorporating local buckling." *J. Struct. Eng.* 126 (3): 341–352. https://doi.org/10.1061/(ASCE)0733-9445(2000)126:3(341).

Varma, A. H. 2000. "Seismic behavior, analysis, and design of high strength square concrete filled steel tube (CFT) columns." Ph.D. thesis, Dept. of Civil and Environmental Engineering, Lehigh Univ.

Wang, Y., P. Chen, C. Liu, and Y. Zhang. 2017. "Size effect of circular concrete-filled steel tubular short columns subjected to axial compression." *Thin-Walled Struct.* 120 (Nov): 397–407. https://doi.org/10.1016/j.tws.2017.09.010.

Wu, M. C., C. C. Chen, and C. C. Chen. 2018. "Size effect on axial behavior of concrete-filled box columns." *Adv. Struct. Eng.* 21 (13): 2068–2078. https://doi.org/10.1177/1369433218766366.

Xiong, M. X. 2012. "Structural behavior of concrete filled steel tubes with high strength materials." Ph.D. thesis, Dept. of Civil and Environmental Engineering, National Univ. of Singapore.

Xiong, M. X., D. X. Xiong, and J. Y. R. Liew. 2017. "Axial performance of short concrete filled steel tubes with high- and ultra-high-strength materials." *Eng. Struct.* 136 (Apr): 494–510. https://doi.org/10.1016/j.engstruct.2017.01.037.

Yamamoto, T., J. Kawaguchi, and S. Morino. 2000. "Experimental study of scale effects on the compressive behavior of short concrete-filled steel tube columns." In *Proc., United Engineering Foundation Conf. on Composite Construction in Steel and Concrete IV (AICE)*, 879–891. Reston, VA: ASCE.

Yan, Y., L. Xu, B. Li, Y. Chi, M. Yu, K. Zhou, and Y. Song. 2019. "Axial behavior of ultra-high performance concrete (UHPC) filled stocky steel tubes with square sections." *J. Constr. Steel Res.* 158 (Jul): 417–428. https://doi.org/10.1016/j.jcsr.2019.03.018.

Zhang, H., and K. J. R. Rasmussen. 2013. "System-based design for steel scaffold structures using advanced analysis." *J. Constr. Steel Res.* 89 (Oct): 1–8. https://doi.org/10.1016/j.jcsr.2013.05.014.